From chemosensing in microorganisms to practical biosensors

Surya K. Ghosh, Tapanendu Kundu, and Anirban Sain
Department of Physics, Indian Institute of Technology, Bombay, Powai, Mumbai 400 076, India
(Received 31 May 2012; revised manuscript received 24 September 2012; published 19 November 2012)

Microorganisms like bacteria can sense concentrations of chemoattractants in their medium very accurately. They achieve this through interaction between the receptors on their cell surfaces and chemoattractant molecules (like sugar). Physical processes like diffusion set some limits on the accuracy of detection, which was discussed by Berg and Purcell in the late seventies. We re-examine their work in order to assess what insight it may offer for making efficient, practical biosensors. We model the functioning of a typical biosensor as a reaction-diffusion process in a confined geometry. Using available data first we characterize the system by estimating the kinetic constants for the binding and unbinding reactions between the chemoattractants and the receptors. Then we compute the binding flux for this system, which Berg and Purcell had discussed. Unlike in microorganisms where the interval between successive measurements determines the efficiency of the nutrient searching process, it turns out that biosensors depend on long time properties like signal saturation time, which we study in detail. We also develop a mean field description of the kinetics of the system.

DOI: 10.1103/PhysRevE.86.051910 PACS number(s): 82.39.−k, 82.40.Ck, 87.15.R−, 87.85.fk

I. INTRODUCTION

Berg and Purcell (BP), in their pioneering article [1] on "physics of chemoreception," had considered how a microorganism could sense concentration of a chemoattractant molecule (say, X) in its surrounding media. They assumed the organism to be a sphere of radius a, immersed in an unbounded liquid medium, and ρ_0 be the far field concentration of X. A simple example could be a bacterium in a dilute sugar (X) solution of local density ρ. The X molecules diffuse and bind to the surface of the sphere, which is assumed to be a perfect sink for X. They solved the diffusion equation, $\partial_t \rho = D\nabla^2\rho$, in the steady state, using spherical coordinates centered at the sphere. Using the boundary conditions $\rho(r = a) = 0$ (i.e., fully absorbing surface) and $\rho(r = \infty) = \rho_0$ (at far field), they found the steady state influx of X molecules (J) integrated over the spherical surface to be $J = 4\pi a D\rho_0$.

We now briefly introduce a typical biosensor and discuss the applicability of these ideas. A biosensor is designed to detect traces of specific biochemicals present in a carrier medium. It can detect, for example, *E. coli* in drinking water [2], hepatitis B surface antigen present in human serum [3], or pollutants in air [4]. The past decade has seen proliferation of such biosensors [5–7] in day-to-day use, mainly due to their (a) quick response time [8] and (b) sensitivity to minute amounts of biomolecules [2]. The particular type of biosensors we discuss here are optics-based chemical sensors, which convert chemical reactions between GaHIgG (X) and HIgG (receptor) molecules into an optical signal, which is then detected using fiber-optics technology. In this sensor, an optical fiber of radius R_i runs along the axis of a cylindrical chamber of radius R_o. The fluid containing the antigen (X) is injected into the annular space between the fiber and the chamber. The surface of the fiber is functionalized by putting on it a certain surface density (σ_0) of antibodies (receptors), which serve as the binding targets for the antigen molecules. Antigens bind to the receptors on the surface of the fiber and absorb evanescent waves generated by the light-carrying fiber. This results in loss of intensity carried by the fiber. For our purpose here, the absorbance ($\mathcal{A}$) of the evanescent waves [9] is proportional to the total bound antigen $\int \sigma dA$ on the fiber surface, where σ is the surface density of bound antigens.

II. MODEL

Such a system can be described, at the continuum level, by reaction diffusion equations [10]. The X molecules bind to the receptors on the fiber surface with a rate ω_b and surface-bound X molecules can also unbind at a rate ω_u, typically much smaller than the binding rate. The values of the kinetic coefficients ω_b and ω_u are unknown a priori, which we determine from experimental data. The bulk concentration of X is ρ, the surface concentration of receptor-bound X molecules is σ, and the surface concentration of receptors is σ_0. Dynamics of ρ follows

$$\frac{\partial \rho}{\partial t} = D\nabla^2\rho - \delta(r - R_i)[\rho(\sigma_o - \sigma)\omega_b - \omega_u\sigma]. \quad (1)$$

We use a cylindrical polar coordinate frame where $\rho = \rho(r,\phi,z,t)$ and $\sigma = \sigma(\phi,z,t)$ with $R_o > r > R_i$. The second term on the right-hand side represents surface reactions at $r = R_i$. The first term in the square brackets describes binding and the second term represents unbinding. Dynamics of σ follows

$$\frac{\partial \sigma}{\partial t} = \rho(\sigma_o - \sigma)\omega_b - \omega_u\sigma. \quad (2)$$

Here ρ is the bulk density in the immediate vicinity of the surface. These equations can be nondimensionalized. We rescale the bulk and the surface densities as $\tilde{\rho} = \frac{\rho}{\rho_0}$ and $\tilde{\sigma} = \frac{\sigma}{\sigma_0}$; and the space and time variables as $\tilde{r} = r/R_i, \tilde{z} = z/L$, and $\tau = \frac{tD}{R_i^2}$. In terms of dimensionless parameters $\tilde{\omega_b} = \omega_b\beta$, $\tilde{\omega_u} = \frac{\omega_u}{\rho_0}\beta$, and $\gamma = \frac{\sigma_0}{\rho_0 R_i}$, where $\beta = \frac{R_i^2}{D}\rho_0$, the equations are

$$\frac{\partial \tilde{\rho}}{\partial \tau} = \tilde{\nabla}^2\tilde{\rho} - \delta(\tilde{r} - 1)\gamma[\tilde{\rho}(1 - \tilde{\sigma})\tilde{\omega_b} - \tilde{\omega_u}\tilde{\sigma},] \quad (3)$$

$$\frac{\partial \tilde{\sigma}}{\partial \tau} = \tilde{\rho}(1 - \tilde{\sigma})\tilde{\omega_b} - \tilde{\omega_u}\tilde{\sigma}. \quad (4)$$

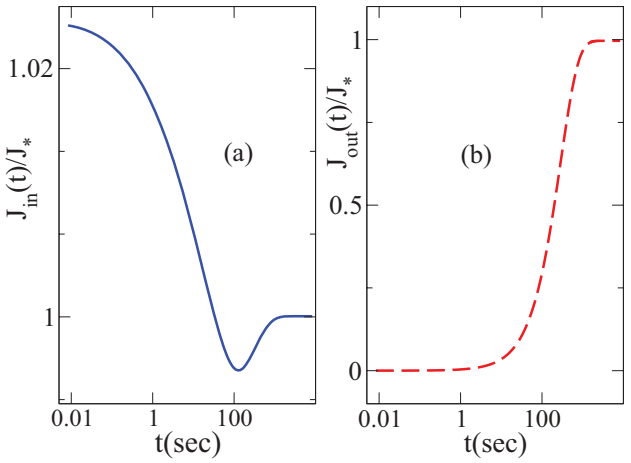

FIG. 1. (Color online) Semilog plot of binding (J_{in}) and unbinding (J_{out}) fluxes (both scaled with the steady state value J_*) as a function of time, at fixed D and $\rho_0(= 0.001$ mg/ml). Values of ω_b and ω_u are same as those found through Fig. 3 (discussed later). J_{in} and J_{out} are plotted separately because their scales of variations are very different, unlike that in Fig. 2.

Superficially the spherical surface of BP is replaced in our biosensor by a cylindrical surface but the big difference is that our system is confined and the total number of antigens is fixed. Thus the steady state here corresponds to a state of dynamic equilibrium when the binding and unbinding at the fiber surface balance each other, making both the bulk and surface concentrations constant is time. Note that although the surface concentration becomes static, the steady state binding (J_{in}) and unbinding (J_{out}) fluxes individually are not zero at the surface (see Figs. 1 and 2, obtained at different values of ω_b) and at large time $J_{\text{in}} = J_{\text{out}} = J_*$. In BP's case, with perfectly absorbing surface, J_{in} is given by the surface integral of the diffusional current $-D\int \vec{\nabla}\rho dA$ onto the absorbing surface (of area A). But for our sensor with finite binding constant, the

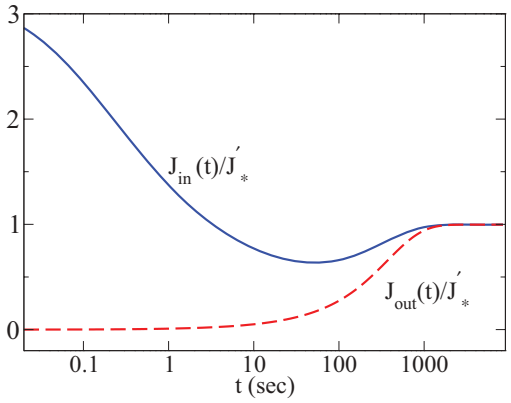

FIG. 2. (Color online) Semilog plot of binding (J_{in}) and unbinding (J_{out}) fluxes (both scaled with the steady state value J'_*) as a function of time. Here we used the same ρ_0, D, and ω_u as in Fig. 1 while ω_b was increased 100 times to reach a steady state value J'_* comparable to J_{BP}. We explain later why this comparison is not very useful due to difference in the boundary conditions in the two problems.

influx $J_{\text{in}} = \int dA\rho(\sigma_o - \sigma)\omega_b$ is computed by integrating the binding term [on the right-hand side of Eq. (2)] over the area A of the fiber surface, and similarly the outflux $J_{\text{out}} = \int dA\omega_u\sigma$ is computed from the unbinding term. We consider the initial condition where at $t = 0$ the system is filled up with a fluid carrying an uniform concentration of X. At $t = 0$ the influx is nonzero as the concentration of X molecules in the vicinity of the fiber surface (ρ_s) is nonzero. On the other hand the outflux is zero at $t = 0$ because there are no bound X molecules at the beginning. BP has considered a perfectly absorbing surface, which can theoretically be attained in the limit $\sigma_0 \to \infty$ and $\omega_u \to 0$. Note that, in Eqs. (1) and (2), when $\sigma_0 \gg \sigma$, the binding term reduces to $\rho_s\sigma_0\omega_b$ and it appears that we do not need ω_b to be infinity in addition. But practically σ_0 is bounded due to the finite size of the receptors. BP had approximated the receptors to occupy a small area with radius $s \sim 10$ Å. For our sensor it amounts to about 10^{13} receptors covering the whole fiber surface. We used this value as the maximum coverage $\sigma_0^{\max}$ for Figs. 1 and 2. To compare with BP's case we focus on the binding flux of X only.

First we adapt BP's general expression [1] for the steady flux $J = 4\pi a D\rho_0$ to our cylindrical geometry. BP had shown that this flux can be calculated for any shape by mapping the steady diffusion equation $\nabla^2\rho = 0$ to the Poisson equation for potential $\nabla^2\phi = 0$, in charge-free space. It can be shown that generally $J = 4\pi C D\rho_0$, where C is the capacitance of a conductor with free charge Q on its surface. Specifically, $C = Q/\phi_\infty$, where ϕ_∞ is the potential difference between the conductor and infinity. For the sensor the cylindrical fiber is the absorbing surface. With a radius $R_i = 0.1$ mm and length $L = 50$ mm (i.e., aspect ration 500) it is as good as a one-dimensional line. For a line charge density λ, extending from $x = -L/2$ to $L/2$, the expression for the potential $\phi(z)$ along the perpendicular bisector, z distance away from the center of the line charge, is $\phi(z) = k\frac{\lambda}{\epsilon_0}\ln\frac{\sqrt{1+(z/L)^2}+1}{\sqrt{1+(z/L)^2}-1}$, where $k = 1/4\pi\epsilon_0$ is the Coulomb force constant. Using the approximation $R_i/L \ll 1$ we get $\phi(R_i) \simeq \frac{2kQ}{L}\ln(2L/R_i)$ and $C \simeq \frac{L}{2}\ln(2L/R_i)$. Thus $J_{BP} \simeq 2\pi DL\rho_0\ln(2L/R_i)$.

To compute the binding flux J_{in} we have to numerically time evolve the dynamical equations [Eqs. (3) and (4). First, to get realistic values for the kinetic coefficients ω_b and ω_u we use experimental data on surface adsorption $\sigma(t)$ versus time from Ref. [11], obtained at two widely different initial bulk densities (a) $\rho_0 = 0.001$ mg/ml and (b) $\rho_0 = 0.1$ mg/ml, and possibly at different surface density of receptors. Note that the nondimensionalized equations (3) and (4) do not explicitly scale with antigen (X) density ρ_0 and therefore these data sets can be treated as independent. Despite the wide difference in ρ_0, the saturation times (τ_0) in the two cases were similar (the symbols in Fig. 3). This could be rationalized by noting that in case-b the fiber was soaked in the receptor solution for 2 hrs while for case-a it was soaked for a very long time (about 16 h). From this information we inferred that in case a $\sigma_0^a = \sigma_0^{\max}$ while for case b $\sigma_0^b < \sigma_0^{\max}$. We choose $D = 10^{-5}$ cm^2/s typical of diffusion of small molecules in water [12,13] (BP also took the same D for their estimates). We had to determine ω_b, ω_u, and σ_0^b by matching our numerical results [from Eqs. (3) and (4)] with the

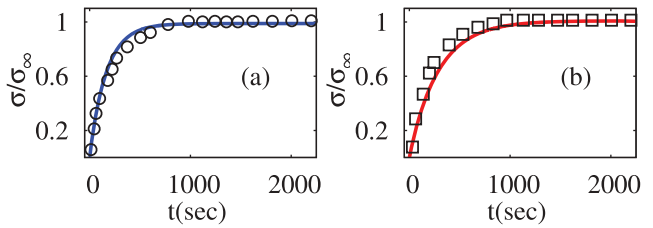

FIG. 3. (Color online) Surface density of bound antigens $\sigma(t)$ vs time. The y axis is scaled with the saturation value $\sigma_\infty = \sigma(t \to \infty)$ since we do not know the proportionality constant connecting experimentally measured absorbance $\mathcal{A}$ and σ. The symbols represent experimental data. In (a) $\rho_0 = 0.001$ mg/ml and in (b) $\rho_0 = 0.1$ mg/ml. The solid lines are from our numerical integration of Eqs. (3) and (4). For (a) we chose $\sigma_0 = 0.08\ \mu\text{g/mm}^2$, i.e., the maximum possible surface coverage. It turns out that a reasonably good match with the two experimental $\sigma(t)$ profiles and with $\sigma^a_\infty/\sigma^b_\infty$ were obtained for $\omega_b = 0.75 \times 10^{-5}\ \mu\text{m}^3/\text{s}$, $\omega_u = 0.35 \times 10^{-2}/\text{s}$, and $\sigma^b_0 = 0.014\ \mu\text{g/mm}^2$, i.e., about 5.5 times less than the maximal coverage.

temporal profiles of $\sigma(t)$ and the ratio $\sigma^a_\infty/\sigma^b_\infty$. We converged to $\omega_b = 0.75 \times 10^{-5}\ \mu\ \text{m}^3\,\text{s}^{-1}$, $\omega_u = 0.35 \times 10^{-2}\,\text{s}^{-1}$, and $\sigma^b_0 = 0.014\ \mu\text{g/mm}^2$. These numbers for ω_u, ω_b appear reasonable when compared to the reaction-diffusion processes on bacterial membranes [10].

As mentioned earlier we used a cylindrical polar coordinate system to discretize the space. Uniform binning was used along z and ϕ, while r coordinate was binned nonuniformly such that the volume of each bin $(rdrd\phi dz)$ remains constant. Reflecting boundary condition was used at the walls of the cylindrical chamber, by ensuring zero currents at the boundaries. We used a uniform distribution of X molecules in the bulk as our initial condition, that is, $\rho(t=0) = \rho_0$ and $\sigma(t=0) = 0$.

We then compute the flux $J_{\text{in}}(t) = \int dA\rho(\sigma_0 - \sigma)\omega_b$, which is the binding term in the right-hand side of Eq. (2), integrated over the cylindrical fiber surface, as a function of time. Interestingly, $J_{\text{in}}(t)$ goes through a minima before it saturates to J_* (see Figs. 1 and 2). We explain the origin of this nonmonotonic behavior later when we study the dynamics in detail. In Fig. 1 the steady state flux J_* is much lower than J_{BP}, while in Fig. 2 it is comparable, but J_* and J_{BP} depend on different sets of parameter values. Both of them are steady state properties, but J_* depends on ω_b, ω_u, σ_0, and ρ_0 while J_{BP} depends on D and ρ_0. This difference arise from the difference in the boundary conditions of a confined versus an unbounded system. Therefore, the comparison is not fair. J_* can be calculated by setting the left-hand side of Eq. (4) to zero and using mass conservation, which is discussed later.

So far we had implicitly assumed that the microorganism can sense the ambient ρ_0 by measuring the influx (J) of X molecules, but BP had also considered the realistic possibility that they can infer ρ_0 by measuring the state of occupation of its surface receptors, that is, density of receptors that are bound to X molecules. In fact this is the recipe which most practical biosensors employ. For example, in our particular sensor $\sigma(t)$ decides the intensity of optical adsorption. In BP's theory a bacteria can sense its $\sigma(t)$ in response to local ρ_0 and decide to move towards or away from the chemoattractant or the chemorepellent, respectively. For a static biosensor $\sigma(t)$ can only increase towards saturation. Since a system takes some time to attain saturation, this measurement process is inherently slow compared to the measurement of instantaneous flux. On the other hand, measurement of any instantaneous variable is prone to fluctuation error whereas long time observables like $\sigma(t \to \infty)$ are more dependable. So the challenge is either to reduce the saturation (waiting time) time or choose an optimum time interval T over which an instantaneous variable like $J(t)$ or $\sigma(t)$ should be measured (so that $\Delta J/J$ or $\Delta\sigma/\sigma$ is small). BP had correctly concluded that a bacteria must employ the second strategy since it has to rapidly change its direction of motion based on comparisons between its successive measurement of $\sigma(t)$. BP had estimated $T \sim 1$ s for *E. coli* bacteria. Recent findings [14] show that bacteria have a very efficient mechanism for amplifying the minute signal generated by binding of external sugar molecules to its receptors. It has the capability of detecting 0.1% change in the attractant density and over four orders of magnitude of sugar concentrations. Reference [15] has shown that for a particular type of biosensor flux detection could be a superior method compared to measuring long time saturation properties. For our sensor, we now investigate in detail how saturation time of the sensor varies in response to ρ_0 and how it can be steered by choosing σ_0.

III. MEAN FIELD THEORY

First we discuss a simple mean field (MF) limit of the dynamics. In the MF approximation we consider the surface concentration to be uniform over the surface of the fiber and the volume concentration to be uniform through out the bulk. Let V_0 be the volume of the annular space and A_0 be the surface area of the fiber. At $t = 0$, $N_0 = \rho_0 V_0$ and later $N_0 = \rho_M V_0 + \sigma_M A_0$, where $\rho_M = \rho_M(t)$ is the mean field density (denoted by subscript M) of X molecules and $\sigma_M = \sigma_M(t)$ is the corresponding surface density of the bound X molecules. In the nondimensional form we have

$$\tilde{\rho}_M = 1 - \alpha\tilde{\sigma}_M, \tag{5}$$

where $\tilde{\rho}_M = \frac{\rho_M}{\rho_0}$, $\tilde{\sigma}_M = \frac{\sigma_M}{\sigma_0}$, and $\alpha = \frac{\sigma_0 A_0}{\rho_0 V_0} = \frac{N_s}{N_0}$. The bulk density ρ_M is homogeneous and slaved by σ_M [via Eq. (5)] so we need to consider only the equation of motion for the surface reaction, namely Eq. (4). By substituting for ρ_M, from Eq. (5) into Eq. (4), and simplifying, we get

$$\frac{d\tilde{\sigma_M}}{d\tau} = \lambda_1\tilde{\sigma}^2_M - \lambda_2\tilde{\sigma}_M + \lambda_3, \tag{6}$$

where $\lambda_1 = \alpha\tilde{\omega}_b$, $\lambda_2 = [(1+\alpha)\tilde{\omega}_b + \tilde{\omega}_u]$, and $\lambda_3 = \tilde{\omega}_b$.

By integrating this equation we get

$$\tau = \int_{\tilde{\sigma}_M(0)=0}^{\tilde{\sigma}_M(\tau)} \left[\frac{d\sigma_M}{\lambda_1\sigma^2_M - \lambda_2\sigma_M + \lambda_3}\right] \tag{7}$$

$$= \frac{2}{i\lambda_R}\left[\tan^{-1}\left(\frac{\lambda_2}{i\lambda_R}\right) - \tan^{-1}\left(\frac{\lambda_2 - 2\lambda_1\tilde{\sigma}_M}{i\lambda_R}\right)\right], \tag{8}$$

where $\lambda_R = \sqrt{\lambda_2^2 - 4\lambda_1\lambda_3}$. By inverting the above equation,

$$\tilde{\sigma}_M(\tau) = \frac{1}{2\lambda_1}\left\{\lambda_2 - \lambda_R \tanh\left[\tanh^{-1}\left(\frac{\lambda_2}{\lambda_R}\right) + \frac{\lambda_R\tau}{2}\right]\right\}. \tag{9}$$

For any set of parameter values, it can be shown that λ_R is always real and we also have $\lambda_2/\lambda_R > 1$. As a result $\tanh^{-1}(\lambda_2/\lambda_R)$ is always a complex number. Using the standard property $\tanh^{-1} x - \coth^{-1} x = i\pi/2$, we can rewrite Eq. (9) as

$$\tilde{\sigma}_M(\tau) = \frac{1}{2\lambda_1}\left[\lambda_2 - \frac{\lambda_R}{\tanh\left[\tanh^{-1}\left(\frac{\lambda_R}{\lambda_2}\right) + \frac{\lambda_R \tau}{2}\right]}\right]. \quad (10)$$

This formula gives excellent fit to the numerical data (not shown here), obtained by integration of Eqs. (3) and (4), at a high value of the diffusion constant, $D = 10^{-3}$ cm^2/s.

The steady state solution ($\tilde{\sigma}_M^s$) can be obtained either by setting $\dot{\tilde{\sigma}}_M = 0$ in Eq. (6) or from the $\tau \to \infty$ limit of Eq. (9). We get $\tilde{\sigma}_M^s = \frac{1}{2\lambda_1}[\lambda_2 - \lambda_R]$.

The mean field approximation will fail if diffusion is not sufficiently fast compared to the time scale at which surface binding reactions cause a depletion in the antigen concentration (ρ). In such a scenario the spatial inhomogeneity in ρ (along r) takes a long time, comparable to the saturation time of the sensor, to homogenize. A better understanding can be gained by comparing the time scales of the three processes: diffusion (t_D), binding (t_b), and unbinding (t_u). We get the individual time scales from Eq. (1) by comparing each term on the right-hand side with that on the left-hand side. For example, $\dot{\rho} \sim D\nabla^2\rho$ gives, by dimensional analysis, $t_D^{-1} \sim \frac{D}{R^2}$. Similarly, $t_b^{-1} \sim \frac{\sigma_0\omega_b}{R}$ and $t_u^{-1} \sim \frac{\sigma_0\omega_b}{\rho_0 R}$. Here we have assumed $R = R_o - R_i$ to be the only relevant length scale. For diffusion, this is the spatial scale of density inhomogeneity. Now, t_b and t_u are the time scales over which density inhomogeneity are created near the fiber due to the surface reactions, while t_D is the time interval during which such inhomogeneities are ironed out. Therefore, mean field approximation requires diffusion to be a faster process, that is, $t_D \ll t_b, t_u$. These inequalities yield the criteria $\frac{\sigma_0\omega_b R}{D} \ll 1$ and $\frac{\sigma_0\omega_u R}{\rho_0 D} \ll 1$. The first inequality suggests that mean field approximation will be correct at high D or low σ_0 values. We have verified these conditions numerically by looking for density inhomogeneity $\rho(r)$ during the transients, in the numerical solution of Eqs. (3) and (4) (see Fig. 4). For example, for $N_s/N_0 = 1, D = 10^{-5}$ cm^2/s the density remains uniform through out, at all times. But when σ_0 is increased by choosing $N_s/N_0 = 10$, strongly inhomogeneous $\rho(r)$ appears (i.e., MF theory fails). Now, in addition, if D is hiked, $\rho(r)$ becomes homogeneous again (graph not shown here). The second inequality suggests that, along with high D and low σ_0, we also need high ρ_0. Only then can both $t_b, t_u \gg t_D$ be satisfied. We have verified this condition on ρ_0 along with similar conditions on ω_b and ω_u resulting from the inequalities. Figure 5 shows a comparison between numerical solution of Eqs. (3) and (4) and mean field results for $\rho_0 = 0.1$ mg/ml and $\sigma_0 = 0.01$ μgm/mm^2, that is, at high ρ_0 and low σ_0. At these parameter values the influx J_{in} does not go through any minima. The reason why the influx J_{in} goes through a minimum in Figs. 1 and 2 is now clear from Fig. 4(b), which shows when $\rho(r)$ becomes inhomogeneous (in the non-MF case) the $\rho(r)$ in the vicinity of the fiber undergoes a dip (triangles) before it becomes uniform (circles) at late times. In the mean field regime the minima is absent because the $\rho(r)$ in the vicinity of the fiber decreases monotonically in time, as is clear from Fig. 4(a).

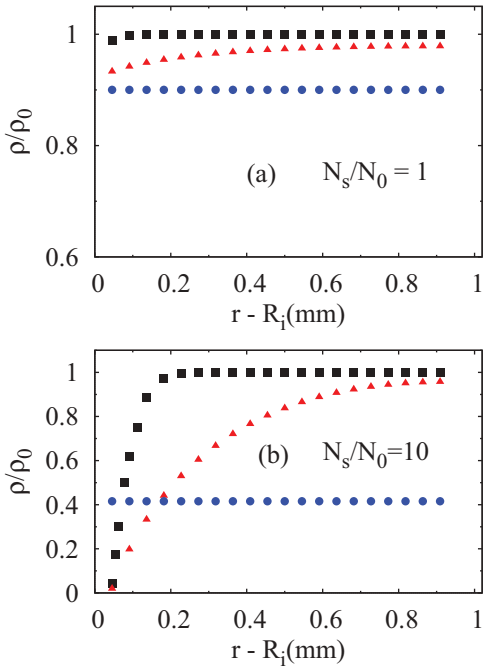

FIG. 4. (Color online) Radial density profile ρ as a function of $r - R_i$ in the bulk, at three different times: right after start (square), at saturation (circle), and at some intermediate time (triangle). Panels (a) and (b) differ in the parameter N_s/N_o (which is proportional to σ_0 at fixed ρ_0). The values of D, ω_b, ω_u were obtained through Fig. 3. Transition from mean field to non-mean-field-type density profile occurs as we go from panels (a) to (b) by increasing N_s/N_o. Note that, at a fixed ρ_0, the fraction of antigens (X) remaining in the bulk can be reduced (consequently the bound proportion can be increased) by increasing N_s/N_o. This is desirable for making the sensor more sensitive, especially when ρ_0 is small.

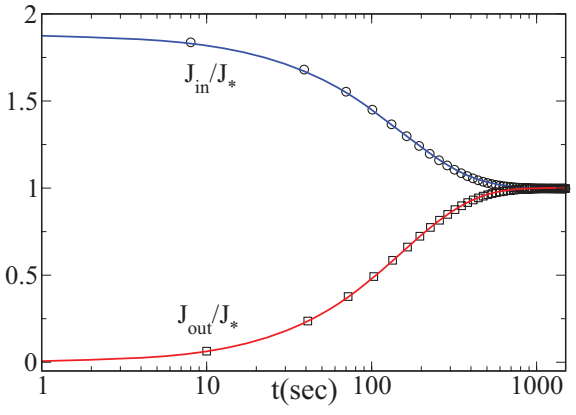

FIG. 5. (Color online) Semilog plot of binding (J_{in}) and unbinding (J_{out}) fluxes as a function of time in the mean field regime (i.e., high ρ_0 and low σ_0 with $N_s/N_0 = 0.05$). The symbols (circles and squares) are obtained from numerical integration of Eqs. (3) and (4), while the solid lines are the corresponding mean field results. Here $\rho_0 = 0.1$ mg/ml, $\sigma_0 = 0.01$ μgm/mm^2, and the values of ω_b and ω_u are the same as those in Fig. 1 (i.e., the values estimated from experimental data).

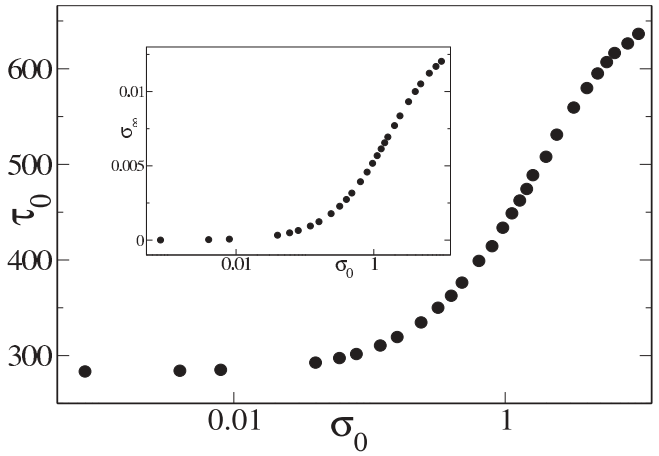

FIG. 6. Semilog plot of saturation time τ_0 (s) vs the density of receptors σ_0 (μg/mm^2). The inset shows saturated signal σ_∞ vs σ_0. We fix ρ_0 at a very low value, 0.001 mg/ml, to test the sensitivity of the sensor. The values of ω_b and ω_u are those estimated before. Both τ_0 and σ_∞ saturate at high values of σ_0, much beyond the maximum surface coverage (0.08 μg/mm^2) considered here. We have explored the seemingly unrealistic $\sigma_0 > \sigma_0^{\max}$ regime here because it may be possible to increase σ_0 by choosing smaller receptor molecules in another system.

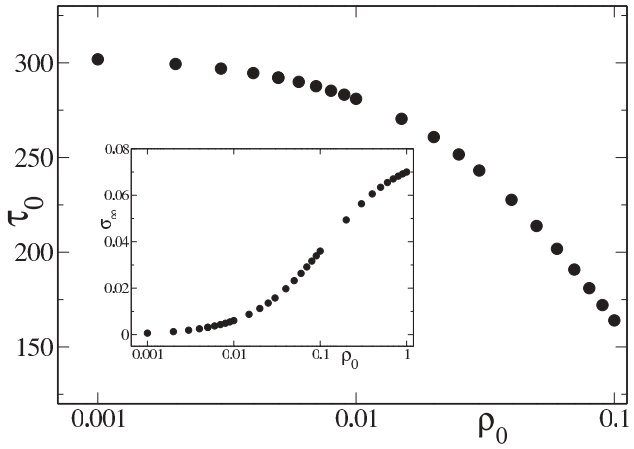

FIG. 7. Semilog plot of saturation time τ_0 (s) vs the density of X molecules ρ_0 (mg/ml). Here σ_0 is held fixed at the maximum surface coverage (0.08 μg/mm^2) in order to maximize the signal. The inset shows that even at this maximum surface coverage the saturated signal σ_∞ drops drastically at low ρ_0.

IV. RESULTS

We now study the general case when MF theory is invalid and thus we have to depend on numerical integration of Eqs. (3) and (4). Our numerical curves for σ versus time, shown in Fig. 3, could be fit to exponential functions like $\sigma(t) = \sigma_\infty(1 - \exp^{-t/\tau_0})$, allowing us to estimate a saturation time scale τ_0 and the saturated value σ_∞ (plotted in Figs. 6 and 7). τ_0 and σ_∞ depend on both σ_0 and ρ_0.

The aim of Figs. 6 and 7 is to identify the regimes where saturation time τ_0 can be reduced and saturated signal σ_∞ can be maximized. For Fig. 6, ρ_0 has been held fixed at a low value, 0.001 mg/ml, while for Fig. 7, σ_0 is fixed at $\sigma_0^{\max} = 0.08\ \mu$g/mm^2. The insets of both the figures show that signal can be enhanced by increasing either ρ_0 or σ_0, which results in decrease or increase of τ_0, respectively. Of course, at high ρ_0 a strong saturated signal can be achieved within a short saturation time, but the sensitivity of a sensor is tested when ρ_0 is small, which we focus on below. For low ρ_0, σ_0 should be maximum to maximize the signal, even at the cost of higher waiting time. Operating near maximum receptor coverage is also necessary, as Fig. 6 shows that the nonlinear response starts to increases near this point. For moderate and high ρ_0, we should choose moderate σ_0 such that τ_0 is not so high and the signal is strong enough. This may appear analogous to the conclusion of BP, where with just a fraction of the cell area ($\sim$1/1000) covered with receptors the steady flux could be as high as $J_{BP}/2$, where J_{BP} is the maximum flux with the fully absorbing surface. The assumption behind this derivation was that the inter-receptor distance is much much greater than the receptor size. In Fig. 6, at 1/10th of the maximum surface coverage (i.e., at $\sigma_0 \sim 0.01\ \mu$g/mm^2) the signal σ_∞ is much weaker compared to that at $\sigma_0^{\max}$. This again highlights the difference between our confined system and the steady state behavior of Berg and Purcell's unbounded system.

In summary, we examined the applicability of Berg and Purcell's ideas to real sensors. In general it turns out that a flux-based sensor is more efficient than one which depends on a long time signal. The flux in our sensor also shows unexpected time variation, which results from competition among different time scales and the extended nature of our system. Another interesting observation is that even at realistic diffusion constant, mean field theory works when ρ_0 is high and σ_0 is small. In general, nonspecific binding of X molecules on the fiber surface can cause complications, but for the system we have chosen here nonspecific binding was verified to be negligible. Further, the surface reactions need not be first order, which we have assumed here. We checked that consideration of second-order binding kinetics does not give any new exotic behavior (e.g., oscillations) but changes the quantitative values of saturation time.

[1] H. Berg and E. Purcell, Biophys. J. **20**, 193 (1977).
[2] T. Geng, J. Uknalis, S. I. Tu, and A. K. Bhunia, Sensors **6**, 796 (2006).
[3] S. Wu *et al.*, Microchim. Acta **166**, 269 (2009).
[4] S. Rodriguez-Mozaz *et al.*, Pure Appl. Chem. **76**, 723 (2004).
[5] D. R. Thevenot, K. Toth, R. A. Durst, and G. S. Wilason, Pure Appl. Chem. **71**, 2333 (1999).
[6] M. D. Marazuela and M. C. Moreno-Bondi, Anal. Bioanal. Chem. **372**, 664 (2002).
[7] A. Sadana and D. Sii, Biosens Bioelectron **7**, 559 (1992).
[8] G. P. Anderson *et al.*, IEEE Eng. Med. Biol. Mag. **13**, 358 (1994).

[9] V. Ruddy, B. D. McGrath, and J. A. Murphy, J. Appl. Phys. **67**, 6070 (1990).
[10] K. C. Huang, Y. Meir, and N. S. Wingreen, Proc. Natl. Acad. Sci. USA **100**, 12724 (2003).
[11] V. V. R. Sai *et al.*, Sensors Actuators: Chem. B **143**, 724 (2010).
[12] R. W. Pastor and M. Karplus, J. Phys. Chem. **92**, 2636 (1988).
[13] D. Brune and S. Kim, Proc. Natl. Acad. Sci. USA **90**, 3835 (1993).
[14] R. M. Weis, Nat. Struct. Mol. Biol. **13**, 382 (2006).
[15] M. K. Muezzinoglu *et al.*, Sensors Actuators B **137**, 507 (2009).